

Temperature Dependence of Low-Frequency Noise Characteristics of $\text{NiO}_x/\beta\text{-Ga}_2\text{O}_3$ p–n Heterojunction Diodes

Subhajit Ghosh, Dinusha Herath Mudiyansele, Fariborz Kargar, Yuji Zhao, Houqiang Fu, and Alexander A. Balandin*

Temperature dependence of the low-frequency electronic noise in $\text{NiO}_x/\beta\text{-Ga}_2\text{O}_3$ p–n heterojunction diodes is reported. The noise spectral density is of the $1/f$ -type near room temperature but shows signatures of Lorentzian components at elevated temperatures and at higher current levels (f is the frequency). It is observed that there is an intriguing non-monotonic dependence of the noise on temperature near $T = 380$ K. The Raman spectroscopy of the device structure suggests material changes, which results in reduced noise above this temperature. The normalized noise spectral density in such diodes is determined to be on the order of 10^{-14} $\text{cm}^2 \text{Hz}^{-1}$ ($f = 10$ Hz) at 0.1 A cm^{-2} current density. In terms of the noise level, $\text{NiO}_x/\beta\text{-Ga}_2\text{O}_3$ p–n diodes perform excellently for new technology and occupy an intermediate position among devices of various designs implemented with different ultra-wide-bandgap semiconductors. The obtained results are important for understanding the electronic properties of $\text{NiO}_x/\beta\text{-Ga}_2\text{O}_3$ heterojunctions and contribute to the development of noise spectroscopy as the quality assessment tool for new electronic materials and device technologies.

emerged as viable options for future power electronic materials and well-established wide-bandgap technologies such as GaN and SiC. In particular, $\beta\text{-Ga}_2\text{O}_3$ has motivated significant research interest owing to easily available high-quality $\beta\text{-Ga}_2\text{O}_3$ substrates and the materials' promising electrical and optical characteristics.^[10,11] Essential device types, including field effect transistors (FETs), and Schottky barrier diodes (SBDs) have been demonstrated.^[12,13] Obtaining p-type Ga_2O_3 to form p–n junction bipolar diodes is difficult.^[14] For this reason, NiO_x has been used as a p-type material to create $\text{NiO}_x/\beta\text{-Ga}_2\text{O}_3$ p–n heterostructures.^[15,16] Bulk NiO_x has a cubic (NaCl-type) structure with a lattice parameter of 0.4177 nm ^[17] and a bandgap, ranging from 3.6 to 4.0 eV .^[18] It is known that NiO_x is a natural p-type UWBG semiconductor, which can be easily deposited into other

n-type semiconductor materials.^[19,20] Such NiO_x -based heterostructures have been used in p–n diodes and other devices.^[21,22] Previous studies on $\text{NiO}_x/\beta\text{-Ga}_2\text{O}_3$ heterostructure diodes reported their promising characteristics, including low leakage currents, high on–off ratio, and low on-resistance.^[23–25] Interestingly, NiO_x is also a well-known spintronic material with a high Néel temperature of 523 K for bulk crystals.^[26]

1. Introduction


In recent years there has been a growing interest in innovative semiconductor heterostructures and electronic technologies to address the ever-increasing industry demands.^[1–6] Ultra-wide-bandgap (UWBG) semiconductor materials have attracted interest for device applications in high-power electronics.^[7–9] Materials such as AlGaIn, AlN, Ga_2O_3 , BN, and diamond

S. Ghosh, F. Kargar, A. A. Balandin
Department of Materials Science and Engineering
University of California
Los Angeles, CA 90095, USA
E-mail: balandin@seas.ucla.edu

S. Ghosh, F. Kargar, A. A. Balandin
Department of Electrical and Computer Engineering
University of California
Riverside, CA 92521, USA

D. H. Mudiyansele, H. Fu
School of Electrical, Computer, and Energy Engineering
Arizona State University
Tempe, AZ 85287, USA

Y. Zhao
Department of Electrical and Computer Engineering
Rice University
Houston, TX 77005, USA

 The ORCID identification number(s) for the author(s) of this article can be found under <https://doi.org/10.1002/aelm.202300501>

© 2023 The Authors. Advanced Electronic Materials published by Wiley-VCH GmbH. This is an open access article under the terms of the [Creative Commons Attribution](https://creativecommons.org/licenses/by/4.0/) License, which permits use, distribution and reproduction in any medium, provided the original work is properly cited.

DOI: 10.1002/aelm.202300501

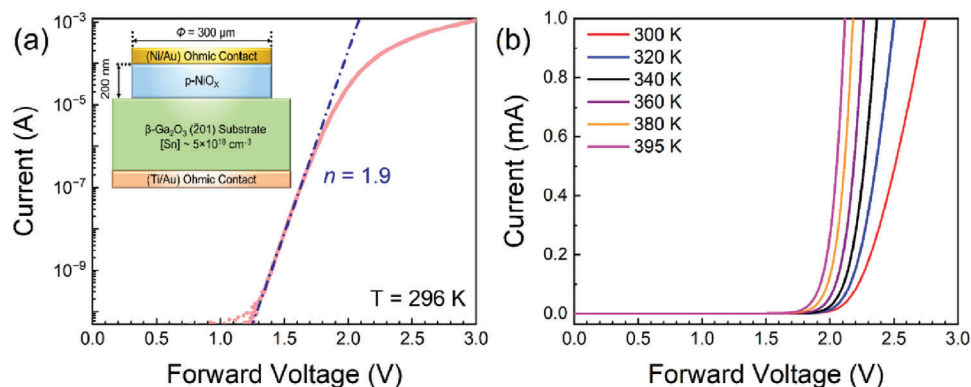


Figure 1. a) Room temperature I – V characteristics of $\text{NiO}_x/\beta\text{-Ga}_2\text{O}_3$ p–n heterojunction diode in the semi-log scale. The extracted ideality factor of the diode is $n = 1.9$. The inset shows a schematic of the device. b) The temperature-dependent I – V characteristics of the device measured between 300 and 395 K. The turn-on voltage (V_T) shifts toward lower forward voltages with increasing temperature.

In this article, we report on the low-frequency noise (LFN) characteristics of $\text{NiO}_x/\beta\text{-Ga}_2\text{O}_3$ p–n heterojunction diodes, focusing on their temperature dependence. The noise measurements are important for understanding the electronic characteristics of $\text{NiO}_x/\beta\text{-Ga}_2\text{O}_3$ heterojunctions, particularly at elevated temperatures. Since UWBG devices are designed to operate at elevated temperatures, the knowledge of high-temperature noise spectra gains extra significance. The most common noise types in semiconductor materials include $1/f$ -type flicker noise and Lorentzian-shaped generation–recombination (G–R) noise.^[27,28] The noise data provides information on charge carrier dynamics and defects, acting as trapping centers. In the case of semiconductor heterostructures, LFN sheds light on the effect of the interfacial states at heterojunctions on the device’s performance. In $\text{NiO}_x/\beta\text{-Ga}_2\text{O}_3$ heterostructures, the interfacial states emerge due to the dangling bond density of the $\beta\text{-Ga}_2\text{O}_3$ substrate plane, which impacts the device performance. Our results contribute to the development of noise spectroscopy as the quality assessment tool for new UWBG device technologies.

2. Experimental Section

For this study, $\text{NiO}_x/\beta\text{-Ga}_2\text{O}_3$ p–n heterostructure diodes were utilized on (201) $\beta\text{-Ga}_2\text{O}_3$ substrate. This type of structure was selected because $\text{NiO}_x/\beta\text{-Ga}_2\text{O}_3$ heterostructures fabricated on (201) substrates have shown high-quality Ohmic contacts, lower turn-on voltage, and better ideality factors. To fabricate the devices, first, (201) $\beta\text{-Ga}_2\text{O}_3$ substrates were obtained from Novel Crystal Technology, Inc. Japan. To clean the substrate, a standard cleaning procedure was implemented, which included sequential cleaning with acetone, isopropyl alcohol, and deionized water, aided by sonication. Next, the back contacts of Ti/Au (20/130 nm) were deposited using electron beam (E-beam) evaporation, followed by rapid thermal annealing at 500 °C in an N_2 environment. Subsequently, standard photolithography techniques were employed to define circular patterns for the deposition of NiO_x and the anode. Using E-beam evaporation, layers of 200 nm NiO_x and the anode Ni/Au (20/130 nm) were deposited, followed by a lift-off process. After that, the devices were subjected to 350 °C annealing in N_2 environment for 1 min. This step was performed to improve the device performance by form-

ing a high-quality Ohmic contact between the Ni/ NiO_x interface and reducing the number of interface states at the $\text{NiO}_x/\beta\text{-Ga}_2\text{O}_3$ heterojunction^[29] (Figure S1, Supporting Information). Additionally, post-annealing, NiO_x displayed a polycrystalline structure, as confirmed through high-resolution transmission electron microscopy (HRTEM) and X-ray diffraction (XRD) analysis. The NiO_x layers were highly doped with a hole density of $>2 \times 10^{18} \text{ cm}^{-3}$.^[30]

The temperature-dependent current–voltage (I – V) measurements were conducted in the vacuum inside a probe station (Lakeshore TTPX) in a 2-terminal configuration using a semiconductor parameter analyzer (Agilent B1500). During the measurements, the sample was placed on top of a sample stage and heated up to 395 K using a temperature controller (Lakeshore Model 336). Figure 1a shows the forward bias I – V characteristics in the semi-log scale of a $\text{NiO}_x/\beta\text{-Ga}_2\text{O}_3$ p–n heterojunction diode with a 300 μm diameter, measured at RT ($T = 296 \text{ K}$). It is noteworthy that the hysteresis observed in the devices, both in terms of capacitance–voltage and forward and reverse I – V characteristics, was minimal as shown in Figure S2 (Supporting Information). This can primarily be attributed to the reduction of trap states at the interface achieved through thermal annealing, as discussed earlier.^[29] The ideality factor, n of the diode device was calculated to be ≈ 1.9 in the low current region. The temperature-dependent characteristics of the diodes were conducted at temperatures in the range from 300 to 395 K, in the heating cycle. It is important to emphasize that within this temperature range, the device behavior remained stable and reproducible as shown in Figure S5 (Supporting Information) for forward I – V measurements conducted between 300 and 423 K at different temperature cycles. The initial I – V curves were retained even after heating and cooling, demonstrating the excellent thermal stability of the p–n heterojunction.^[31] Figure 1b shows the forward-bias I – V s of the diode at different temperatures. The turn-on voltage, V_T , of the diode, decreases linearly as its temperature increases. The decrease in V_T at elevated temperatures is attributed to the decrease in the depletion width at the heterojunction owing to the thermal diffusion of holes from the p- NiO_x layer.^[32]

The LFN measurements were conducted inside the probe station chamber under a high vacuum following a standard protocol.^[33,34] The noise measurement system consists of the

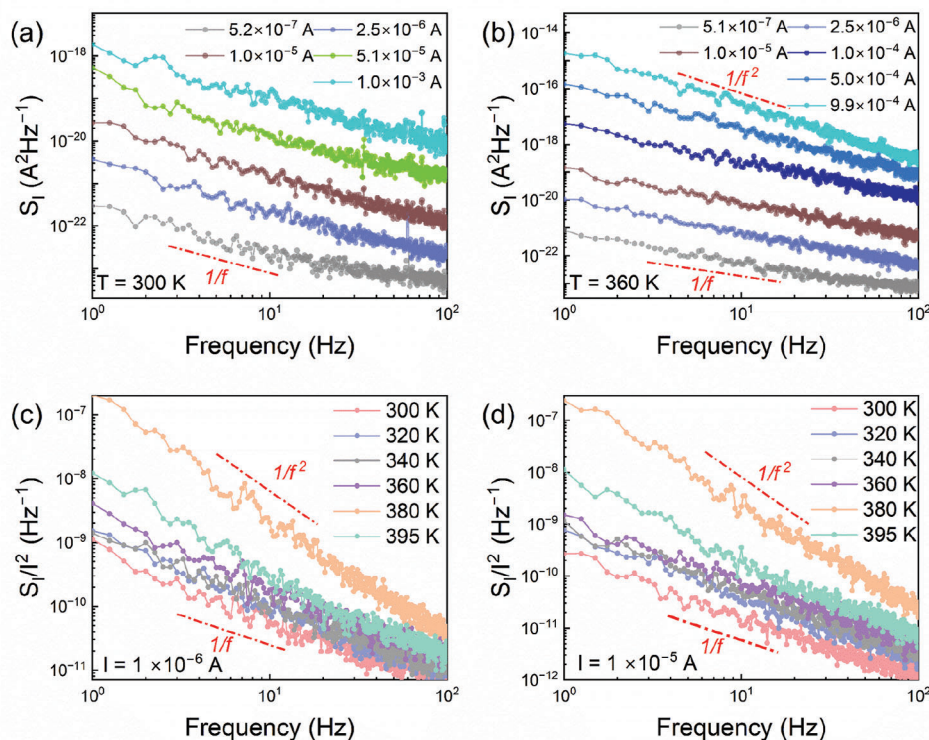


Figure 2. a) The current noise spectral density, S_I , as a function of frequency, f , measured at $T = 300$ K for different forward current values. The noise spectra are of $1/f$ type for all currents. b) The S_I versus f characteristics for different temperatures of 360 K. The noise spectra remain $1/f$ at lower and intermediate current levels but change to $1/f^2$ Lorentzian type at higher currents, above $I = 100 \mu\text{A}$. c) The normalized noise spectral density, S_I/I^2 , as a function of frequency, f , at current $I = 1 \mu\text{A}$ at different temperatures. The noise spectra change from $1/f$ at 300 K to $1/f^2$ at higher temperatures. d) The corresponding temperature-dependent S_I/I^2 versus f for the current $I = 10 \mu\text{A}$.

device under test connected in series to a load resistor and powered by a low-noise dc battery used as a voltage source. A potentiometer was connected to control the voltage drop across the circuit. During the noise measurements at each temperature point, the output voltage fluctuation, ΔV , was transferred to the low-noise voltage preamplifier (SR 560) which amplified the signal. The amplifier was connected to a dynamic signal analyzer (Photon+) to convert the time domain voltage fluctuation signal to the corresponding frequency-dependent voltage spectral density, S_V . For noise data analysis, the obtained voltage spectral density, S_V , was converted to the corresponding current spectral density, S_I . Further details of the noise measurement protocol, in the context of other materials and devices, can be found in prior reports.^[33–35]

3. Results and Discussion

The LFN characteristics of the diode are presented in Figure 2a–d at varying forward currents and different temperatures. Figure 2a shows the current spectral density, S_I , as a function of frequency, f , at different diode current regimes, at 300 K. The noise spectra show a consistent $1/f$ flicker-type noise dependence at all the measured currents. Similar $1/f$ power law-dependent noise behavior was observed at varying device current levels at the next measured temperatures of 320 and 340 K (Figure S6a,b, Supporting Information). The nature of the noise behavior starts to

change at 360 K as shown in Figure 2b. In this temperature, the noise spectra at the lower current regimes followed $1/f$ dependence as observed previously. However, the noise behavior changes to the $1/f^2$ -type noise at higher current levels (starting from $I = 5 \times 10^{-4}$ A). The noise behavior at 380 K remains $1/f^2$ Lorentzian type at all measured current levels as shown in Figure S6c (Supporting Information). At 395 K, at lower current, the noise spectra move toward $1/f$ dependence again. The $1/f^2$ -type spectrum indicates the tail of the Lorentzian, characteristic of the G–R noise. The Lorentzian can indicate either a dominant trap with a specific time constant or a phase transition.^[27] To better understand the change in the noise characteristics with temperature and current we plotted the normalized current spectral density, S_I/I^2 , as a function of frequency, f , at constant diode currents with varying temperatures. Figure 2c presents S_I/I^2 for elevated temperatures at the fixed current level of $I = 1 \times 10^{-6}$ A. The noise shows $1/f$ dependence at temperatures up to 360 K. At 380 K the noise spectrum changes to the $1/f^2$ dependence with the noise level increased by several orders of magnitude as compared to the noise at lower temperatures. At the next temperature of 395 K, the noise spectrum becomes the $1/f$ -type again and decreases in the overall level. The non-monotonic dependence of noise on temperature was also observed at other current levels as shown in Figure 2d for $I = 1 \times 10^{-5}$ A. We also observed similar noise behavior at higher currents of $I = 1 \times 10^{-4}$ A and $I = 5 \times 10^{-4}$ A in the ON state of the diode as shown in Figure S7

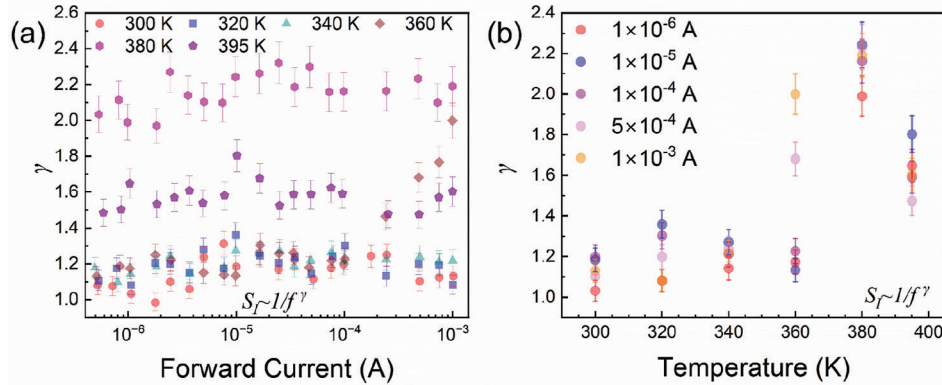


Figure 3. a) The dependence of the noise parameter, γ , on the forward currents at different temperatures. The γ value stays between 0.9 and 1.3 in the lower temperature region but moves toward a higher value of ≈ 2 or more at 380 K due to the emergence of the Lorentzian component. b) The γ parameter dependence on temperature at different current levels.

(Supporting Information). A possible origin of this intriguing non-monotonic noise behavior with temperature is discussed below.

It is known that flicker noise is seldom exactly $1/f$ type. More often its spectrum is described as $S_I = 1/f^\gamma$, where γ is the noise parameter. The deviation of the γ parameter from unity and its dependence on temperature and current are considered to be important metrics for semiconductor devices.^[27] **Figure 3a** provides the extracted γ values as a function of the forward bias current, I , at different temperatures for a NiO_x/β-Ga₂O₃ p-n heterojunction diode. The γ value varies between 0.9 and 1.3 across the measured currents at temperatures between 300 and 340 K. At 360 K the γ parameter sharply increases to ≈ 2 at higher currents. At 380 K, the γ parameter is between 1.9 and 2.3 owing to the emergence of the G–R features. The extracted γ value drops to ≈ 1.6 at 395 K which indicates a non-monotonic change in noise spectral shape. One can see in **Figure 3b** that the γ remains close to ≈ 1 at lower temperatures up to 360 K, and low current levels. It increases sharply to ≈ 2 at 380 K and drops again at 395 K. Previously, a strong dependence of the γ parameter on bias voltage was interpreted as evidence of the non-uniform distribution of traps in space and energy.^[36,37] We have a weak current dependence on the γ parameter. The deviation γ from unity and sharp increase

at 380 K are likely indicating some changes in the material or transport regime as discussed below.

In **Figure 4a** we present the current spectral density, S_I , measured at $f = 10$ Hz as a function of forward current, I , at different temperatures. At smaller temperatures, the noise behavior follows S_I – I linear dependence. Such noise behavior is typical for diode devices and has previously been observed for other diode technologies.^[33,38,39] Interestingly, $S_I(I)$ dependence becomes closer to quadratic, S_I – I^2 , at 380 K. The quadratic behavior is expected for linear resistors and can also be found in diodes in certain transport regimes.^[34,35,40,41] **Figure 4b** shows the normalized noise spectral density, S_I/I^2 , at $f = 10$ Hz as a function of temperature for different currents. At lower currents, the normalized noise level remains within a specific range till 360 K and increases sharply to its maximum value at 380 K before dropping to lower levels at 395 K.

The non-monotonic noise dependence on temperature is intriguing (see **Figure 4b**). In the I – V characteristics, we did not observe any anomaly at 380 K (see **Figure 1b**), which could explain the noise peak around that temperature. The noise increases at 380 K is accompanied by the appearance of the Lorentzian features, i.e., $1/f^2$ tail. It is known that LFN can be extremely sensitive to various structure, morphological, defect density, and phase

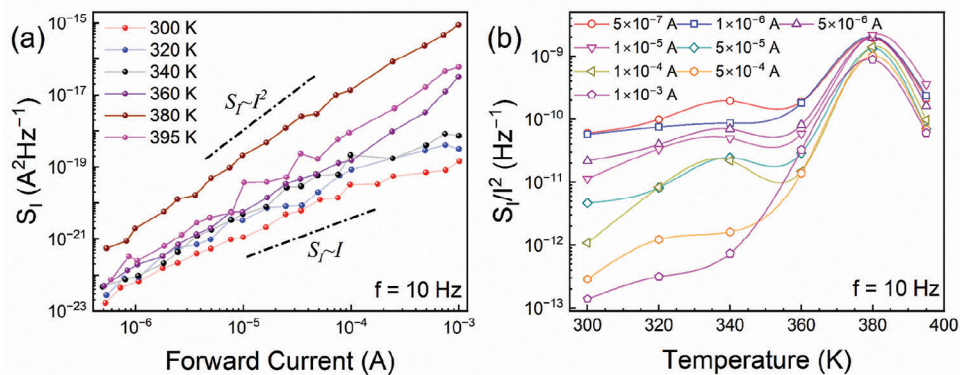


Figure 4. a) The current noise spectral density, S_I , at $f = 10$ Hz as a function of the forward current, I , at elevated temperatures. The noise initially follows S_I – I dependence but changes to S_I – I^2 behavior at higher temperatures. b) The normalized current noise spectral density, S_I/I^2 , as a function of temperature, T , at different current values.

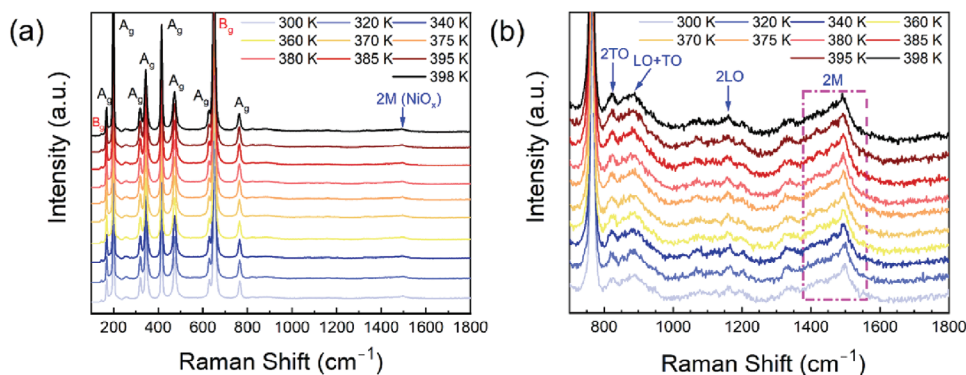


Figure 5. a) Raman spectra of the $\text{NiO}_x/\beta\text{-Ga}_2\text{O}_3$ diode measured in the temperature range between 300 and 398 K. The Raman spectra are dominated by the A_g and B_g vibrational modes of $\beta\text{-Ga}_2\text{O}_3$ substrate in the frequency range between 100 and 800 cm^{-1} . A small hump around 1500 cm^{-1} is assigned to the two-magnon (2 M) Raman peak of the antiferromagnetic NiO_x layer. b) The low-intensity peaks in the high-frequency region originate from the $p\text{-NiO}_x$ layer. One can see the second-order LO and TO phonon modes and the 2 M peak, which remains visible in the entire measured temperature range.

changes in the material. While I - V characteristics do not show any changes, the current fluctuations, i.e., noise, can reveal even small structural or morphological variations. The LFN measurements were used to detect various phase transitions in different materials, including charge-density-wave phase transitions^[42-44] and magnetic phase transitions in AFM materials.^[45] The noise spectra at the transition temperatures generally show an increase in the noise level and an emergence of the pronounced Lorentzian features. Bulk single crystal NiO_x reveals a magnetic phase transition from the AFM to the paramagnetic (PM) phase at the Néel temperature of 523 K.^[26] However, the Néel temperature of NiO_x can vary significantly depending on the size of NiO polycrystalline grains, morphology, stoichiometry, and lattice defects.^[46] It was found that NiO_x nanoparticles, with grain sizes of $\approx 100\text{ nm}$, have substantially lower Néel temperature, which can decrease even below 300 K as evidenced by the disappearance of the two-magnon peak in the Raman spectra.^[47]

In order to detect any possible modifications in the material of the device upon heating, we conducted Raman spectroscopy measurements in the corresponding temperature range between 300 and 398 K. The Raman measurements were conducted in the conventional backscattering configuration using $\lambda = 488\text{ nm}$ laser excitation with 1800 g mm^{-1} grating and a $50\times$ objective (Renishaw In-Via). The laser power was kept at $\approx 3\text{ mW}$ to avoid local Joule heating in the device structure from the excitation laser. The diode was placed on top of a heating stage (Linkam THMS600) so that the Raman measurements can be conducted at elevated temperatures. **Figure 5a** shows the temperature-dependent Raman spectra between 100 and 1800 cm^{-1} . The spectra are dominated by intense low-frequency phonon peaks from the $\beta\text{-Ga}_2\text{O}_3$ substrate. Only a small hump related to the two-magnon (2 M) peak from the NiO_x layer can be observed. The wave numbers of the observed spectral features between 100 and 800 cm^{-1} are in good agreement with the literature on $\beta\text{-Ga}_2\text{O}_3$ Raman modes.^[48-50] **Figure 5b** shows the low-intensity peaks from the NiO_x layer found between 700 and 1800 cm^{-1} . The spectra in that region contain the second-order LO and TO vibrational modes as well as the 2 M peak related to the NiO material.^[26,51] One can see that the 2 M peak exists in the entire examined temperature range. This suggests that the NiO_x layer

remains in the AFM phase and the peak and Lorentzian spectral features observed in noise spectra are likely associated with other changes in materials used in $\text{NiO}_x/\beta\text{-Ga}_2\text{O}_3$ p-n heterojunction diodes.

To assess the possibility of the change in material characteristics, we plotted the Raman shifts and intensity as the functions of temperature for several peaks associated with the $\beta\text{-Ga}_2\text{O}_3$ substrates (see **Figure 6a-d**). The Raman peak frequencies red-shift with increasing temperature as expected for conventional semiconductor materials. The trend experiences a clear change at temperatures above 360 K (**Figure 6a-b**). The temperature coefficients for different Raman peaks are different but the behavior around 360 K is consistent (see Additional Data of Supporting Information). We also observed a non-monotonic dependence of the peak intensities with a maximum value near 380 K (**Figure 6c-d**). One can recall that the noise level also reached its maximum at $\approx 380\text{ K}$ and then decreased (see **Figure 4b**). The non-monotonic trend in the Raman intensity and the changes in the Raman temperature coefficients for the phonon modes associated with $\beta\text{-Ga}_2\text{O}_3$ and $\text{NiO}_x/\beta\text{-Ga}_2\text{O}_3$ heterointerface suggest a possibility of material changes at these temperatures, which result in reduced defects or improvement of the crystalline or morphological structure at $T > 380\text{ K}$. We also excluded the possibility of the energy bandgap change in NiO_x material contributing to the non-monotonic behavior of the noise at higher temperatures. In our estimate, the change in bandgap for the NiO_x layer between 300 and 400 K is less than 0.1 eV ($E_g(300\text{ K}) = 3.84\text{ eV}$ and $E_g(400\text{ K}) = 3.76\text{ eV}$).^[52]

A recent study has shown that rapid thermal annealing of $\text{NiO}_x/\beta\text{-Ga}_2\text{O}_3$ heterojunction diodes can provide significant improvement in the quality of the p-n diode interface, accompanied by a decrease in the interfacial defect states acting as recombination centers.^[53] In the reported study, annealing was performed at $225\text{ }^\circ\text{C}$ in an N_2 atmosphere to improve $\text{Ga}_2\text{O}_3/\text{NiO}$ interface quality.^[53] The latter supports our suggestions that heating the device externally and increasing the temperature further due to the local Joule heating can change the material quality and result in the observed noise behavior. The emergence of the G-R Lorentzian bulges at $T \approx 380\text{ K}$ can indicate the onset of changes in the material, followed by the noise decrease at higher

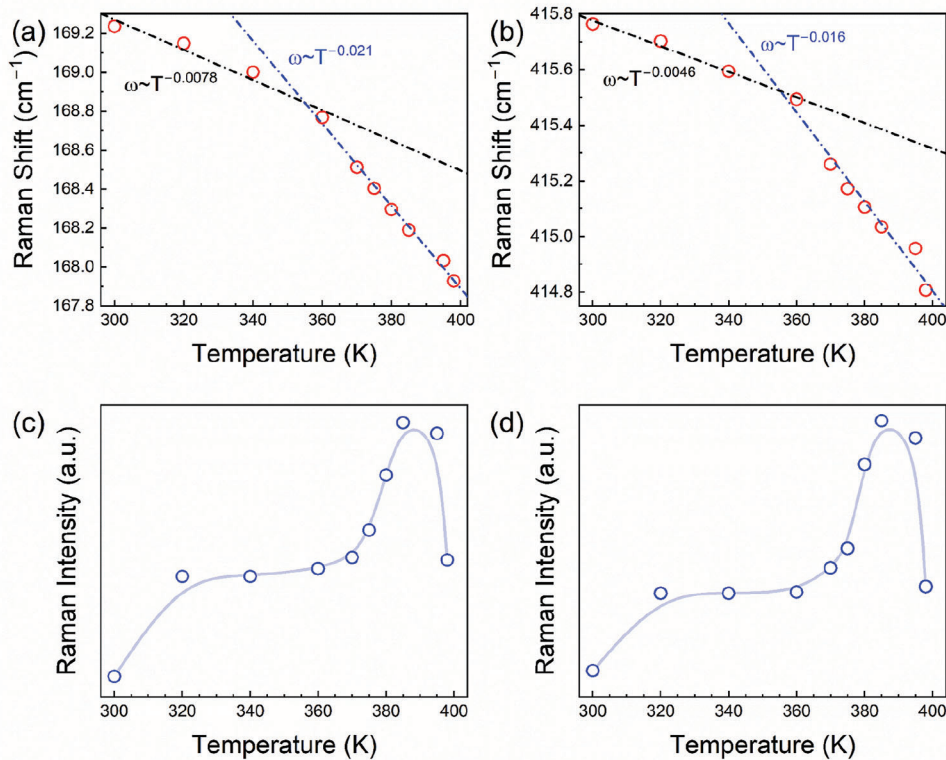


Figure 6. a) Raman frequency as a function of temperature for the A_g peak at $\approx 169\text{ cm}^{-1}$ from the $\beta\text{-Ga}_2\text{O}_3$ substrate. The frequency decreases with increasing temperature but changes more rapidly beyond 360 K. b) The same as in (a) plotted for the A_g Raman peak at $\approx 415\text{ cm}^{-1}$. Similar to A_g peak shown in (a), the rate of change of the Raman frequency is larger after 360 K. c) The Raman peak intensity as a function of temperature for the A_g peak at $\approx 169\text{ cm}^{-1}$. The Raman intensity shows a non-monotonic dependence with the maximum value at $T = 385\text{ K}$. d) The same as in (c) plotted for the A_g Raman peak at $\approx 415\text{ cm}^{-1}$.

temperatures because of the reduced number of defects contributing to $1/f$ noise.

Another interesting feature in the noise response of $\text{NiO}_x/\beta\text{-Ga}_2\text{O}_3$ p-n heterojunction diodes is related to the noise spectral density dependence on current. It changes from linear, $S_I \sim I$, around 300 K to quadratic, $S_I \sim I^2$, near 380 K. It is not uncommon to observe distinct $S_I(I)$ behavior at different current regimes, as observed for other diode technologies.^[33–35,41,54,55] Such noise behavior is attributed to different transport mechanisms dominating at different current regimes. It has been reported that the main transport mechanisms in $\text{NiO}_x/\beta\text{-Ga}_2\text{O}_3$ heterojunction diode are the interface recombination current or the trap-assisted tunneling current.^[56] An interplay of these mechanisms may result in the changed noise spectral density dependence on

current. A similar evolution of the $S_I(I)$ behavior was reported for other heterojunction devices.^[57,58] For practical applications, it is important to compare the noise level in one electronic material and device type with that one in other electronic materials and devices. The noise level can be the overall indicator of the material quality and the maturity of the UWBG device technology. In Table 1, we provide such a comparison for wide-bandgap semiconductor diode technologies using our own and other reported data. One can see that the Normalized noise spectral density of $\text{NiO}_x/\beta\text{-Ga}_2\text{O}_3$ p-n heterojunction diodes is on the order of $10^{-14}\text{ cm}^2\text{ Hz}^{-1}$ ($f = 10\text{ Hz}$) at 0.1 A cm^{-2} current density, which is higher than that in GaN P-I-N diodes and GaN/AlGaIn Schottky diodes, but lower than that in AlGaO Schottky diodes, diamond diodes, and comparable to the noise level in SiC p-n diodes.

Table 1. Comparison of noise level in wide-bandgap semiconductor diode technologies.

Device type	$S_I [\text{A}^2\text{Hz}^{-1}] [f = 10\text{ Hz}, I = 10^{-6}\text{ A}]$	$S_I/I^2 \times \text{Area} [\text{cm}^2\text{Hz}^{-1}] [f = 10\text{ Hz}]$	Refs.
$\text{NiO}_x/\beta\text{-Ga}_2\text{O}_3$ p-n diode	6.5×10^{-23}	4×10^{-14}	This work
GaN P-I-N diode	$10^{-20}\text{--}10^{-22}$	10^{-15}	[33]
Diamond diode	$10^{-17}\text{--}10^{-18}$	$10^{-10}\text{--}10^{-12}$	[34]
AlGaO Schottky diode	1.5×10^{-17}	10^{-12}	[35]
GaN/AlGaIn Schottky diode	10^{-21}	4×10^{-15}	[41]
SiC p-n diode	10^{-23}	6×10^{-14}	[54]

4. Conclusion

In summary, we reported on the temperature dependence of LFN in NiO_x/β-Ga₂O₃ p–n heterojunction diodes and compared the noise level in such devices with that in other UWBG technologies. The normalized noise spectral density in NiO_x/β-Ga₂O₃ p–n heterojunction diodes is higher than that in GaN P–I–N diodes and GaN/AlGaN Schottky diodes, but lower than that in AlGaO Schottky diodes, diamond diodes, and comparable to the noise level in SiC p–n diodes. We observed an intriguing non-monotonic dependence of the noise on temperature, which was attributed to the material characteristic changes. The Raman spectroscopy of the device structure suggests material changes, which results in reduced noise above this temperature. The obtained results are important for understanding the electronic characteristics of NiO_x/β-Ga₂O₃ heterojunctions and contribute to the development of noise spectroscopy as the quality assessment tool for new device technologies.

Supporting Information

Supporting Information is available from the Wiley Online Library or from the author.

Acknowledgements

The work was supported by ULTRA, an Energy Frontier Research Center (EFRC) funded by the U.S. Department of Energy, Office of Science, Basic Energy Sciences under Award # DE-SC0021230.

Author Contributions

S.G. and D.H.M. contributed equally to this work. A.A.B. coordinated the project and led the data analysis and manuscript preparation. S.G. conducted I–Vs, noise, and Raman measurements and contributed to the data analysis; D.H.M. fabricated p–n heterojunction diodes and measured I–Vs; Y.Z. and H.F. supervised device fabrication; F.K. contributed to the diode I–V and noise and Raman data analysis. All authors contributed to the manuscript preparation.

Conflict of Interest

The authors declare no conflict of interest.

Data Availability Statement

The data that support the findings of this study are available from the corresponding author upon reasonable request.

Keywords

1/f noise, flicker noise, p–n diodes, wide bandgap semiconductors

Received: July 25, 2023

Revised: October 26, 2023

Published online: November 29, 2023

- [1] J. Y. Tsao, S. Chowdhury, M. A. Hollis, D. Jena, N. M. Johnson, K. A. Jones, R. J. Kaplar, S. Rajan, C. G. Van De Walle, E. Bellotti, C. L. Chua, R. Collazo, M. E. Coltrin, J. A. Cooper, K. R. Evans, S. Graham, T. A. Grotjohn, E. R. Heller, M. Higashiwaki, M. S. Islam, P. W. Juodawlkis, M. A. Khan, A. D. Koehler, J. H. Leach, U. K. Mishra, R. J. Nemanich, R. C. N. Pilawa-Podgurski, J. B. Shealy, Z. Sitar, M. J. Tadjer, et al., *Adv. Electron. Mater.* **2018**, *4*, 1600501.
- [2] K. Kaneko, Y. Masuda, S. I. Kan, I. Takahashi, Y. Kato, T. Shinoh, S. Fujita, *Appl. Phys. Lett.* **2021**, *118*, 102104.
- [3] M. Higashiwaki, R. Kaplar, J. Pernot, H. Zhao, *Appl. Phys. Lett.* **2021**, *118*, 200401.
- [4] J. He, W. C. Cheng, Q. Wang, K. Cheng, H. Yu, Y. Chai, *Adv. Electron. Mater.* **2021**, *7*, 2001045.
- [5] Y.-Y. Zhang, S. An, Y. Zheng, J. Lai, J. H. Seo, K. H. Lee, M. Kim, *Adv. Electron. Mater.* **2022**, *8*, 2100652.
- [6] J. Shi, J. Zhang, L. Yang, M. Qu, D. C. Qi, K. H. L. Zhang, *Adv. Mater.* **2021**, *33*, 202006230.
- [7] T. Razzak, H. Xue, Z. Xia, S. Hwang, A. Khan, W. Lu, S. Rajan, in *2018 IEEE MTT-S Int. Microwave Workshop Series on Advanced Materials and Processes for RF THz Applications (IMWS-AMP)*, IEEE, Ann Arbor, MI, USA **2018**.
- [8] Z. Zhang, W. Zhang, Q. Jiang, Z. Wei, Y. Zhang, H. L. You, M. Deng, W. Zhu, J. Zhang, C. Zhang, Y. Hao, *IEEE Electron Device Lett.* **2020**, *41*, 1532.
- [9] P. A. Butler, W. M. Waller, M. J. Uren, A. Allerman, A. Armstrong, R. Kaplar, M. Kuball, *IEEE Electron Device Lett.* **2018**, *39*, 55.
- [10] S. Rafique, L. Han, H. Zhao, *ECS Trans.* **2017**, *80*, 203.
- [11] M. Higashiwaki, *AAPPS Bull.* **2022**, *32*, 3.
- [12] M. Higashiwaki, K. Sasaki, A. Kuramata, T. Masui, S. Yamakoshi, *Appl. Phys. Lett.* **2012**, *100*, 13504.
- [13] J. Yang, S. Ahn, F. Ren, S. J. Pearton, S. Jang, A. Kuramata, *IEEE Electron Device Lett.* **2017**, *38*, 906.
- [14] S. J. Pearton, J. Yang, P. H. Cary, F. Ren, J. Kim, M. J. Tadjer, M. A. Mastro, *Appl. Phys. Rev.* **2018**, *5*, 011301.
- [15] X. Lu, Y. Deng, Y. Pei, Z. Chen, G. Wang, *J. Semicond.* **2023**, *44*, 061802.
- [16] H. Gong, X. Chen, Y. Xu, Y. Chen, F. Ren, B. Liu, S. Gu, R. Zhang, J. Ye, *IEEE Trans. Electron Devices* **2020**, *67*, 3341.
- [17] I. Hotovy, J. Huran, L. Spiess, *J. Mater. Sci.* **2004**, *39*, 2609.
- [18] Z. T. Khodair, B. A. Ibrahim, M. K. Hassan, *Mater. Today Proc.* **2020**, *20*, 560.
- [19] G. Turgut, S. Duman, *J. Alloys Compd.* **2016**, *664*, 547.
- [20] Y. Luo, B. Yin, H. Zhang, Y. Qiu, J. Lei, Y. Chang, Y. Zhao, J. Ji, L. Hu, *J. Mater. Sci. Mater. Electron.* **2016**, *27*, 2342.
- [21] H. Ohta, M. Hirano, K. Nakahara, H. Maruta, T. Tanabe, M. Kamiya, T. Kamiya, H. Hosono, *Appl. Phys. Lett.* **2003**, *83*, 1029.
- [22] L. Li, J. Chen, Z. Liu, T. Que, X. Gu, L. He, Y. Liu, *Appl. Surf. Sci.* **2019**, *475*, 1043.
- [23] X. Lu, X. Zhou, H. Jiang, K. W. Ng, Z. Chen, Y. Pei, K. M. Lau, G. Wang, *IEEE Electron Device Lett.* **2020**, *41*, 449.
- [24] Y. Lv, Y. Wang, X. Fu, S. Dun, Z. Sun, H. Liu, X. Zhou, X. Song, K. Dang, S. Liang, J. Zhang, H. Zhou, Z. Feng, S. Cai, Y. Hao, *IEEE Trans. Power Electron.* **2021**, *36*, 6179.
- [25] C. Wang, H. Gong, W. Lei, Y. Cai, Z. Hu, S. Xu, Z. Liu, Q. Feng, H. Zhou, J. Ye, J. Zhang, R. Zhang, Y. Hao, *IEEE Electron Device Lett.* **2021**, *42*, 485.
- [26] E. Aytan, B. Debnath, F. Kargar, Y. Barlas, M. M. Lacerda, J. X. Li, R. K. Lake, J. Shi, A. A. Balandin, *Appl. Phys. Lett.* **2017**, *111*, 252402.
- [27] A. A. Balandin, *Noise and Fluctuations Control in Electronic Devices*, American Scientific Publishers, California, USA, **2002**, p. 258.
- [28] A. A. Balandin, *Nat. Nanotechnol.* **2013**, *8*, 549.
- [29] W. Hao, Q. He, K. Zhou, G. Xu, W. Xiong, X. Zhou, G. Jian, C. Chen, X. Zhao, S. Long, *Appl. Phys. Lett.* **2021**, *118*, 043501.

- [30] D. H. Mudiyansele, R. Mandia, D. Wang, J. Adivarahan, Z. He, K. Fu, Y. Zhao, M. R. McCartney, D. J. Smith, H. Fu, *Appl. Phys. Express* **2023**, *16*, 094002.
- [31] J. Zhang, P. Dong, K. Dang, Y. Zhang, Q. Yan, H. Xiang, J. Su, Z. Liu, M. Si, J. Gao, M. Kong, H. Zhou, Y. Hao, *Nat. Commun.* **2022**, *13*, 3900.
- [32] J. S. Li, C. C. Chiang, X. Xia, F. Ren, S. J. Pearton, *J. Vacuum Sci. Technol. A* **2022**, *40*, 063407.
- [33] S. Ghosh, K. Fu, F. Kargar, S. Rumyantsev, Y. Zhao, A. A. Balandin, *Appl. Phys. Lett.* **2021**, *119*, 243505.
- [34] S. Ghosh, H. Surdi, F. Kargar, F. A. Koeck, S. Rumyantsev, S. Goodnick, R. J. Nemanich, A. A. Balandin, *Appl. Phys. Lett.* **2022**, *120*, 62103.
- [35] S. Ghosh, D. H. Mudiyansele, S. Rumyantsev, Y. Zhao, H. Fu, S. Goodnick, R. Nemanich, A. A. Balandin, *Appl. Phys. Lett.* **2023**, *122*, 212109.
- [36] Z. Celik-Butler, T. Y. Hsiang, *Solid. State. Electron.* **1987**, *30*, 419.
- [37] A. Balandin, S. V. Morozov, S. Cai, R. Li, K. L. Wang, G. Wijeratne, C. R. Viswanathan, *IEEE Trans. Microw. Theory Techniques* **1999**, *47*, 1413.
- [38] T. Li, D. J. H. Lambert, M. M. Wong, C. J. Collins, B. Yang, A. L. Beck, U. Chowdhury, R. D. Dupuis, J. C. Campbell, *IEEE J. Quantum Electron.* **2001**, *37*, 538.
- [39] Z. Khurelbaatar, Y.-H. Kil, K.-H. Shim, H. Cho, M.-J. Kim, S.-N. Lee, J.-C. Jeong, H. Hong, C.-J. Choi, *Superlattices Microstruct.* **2016**, *91*, 306.
- [40] X. Y. Chen, A. Pedersen, A. D. Van Rheenen, *Microelectron. Reliab.* **2001**, *41*, 105.
- [41] G. Cywinski, K. Szkudlarek, P. Kruszewski, I. Yahnuk, S. Yatsunenko, G. Muziol, C. Skierbiszewski, W. Knap, S. L. Rumyantsev, *Appl. Phys. Lett.* **2016**, *109*, 033502.
- [42] S. Ghosh, F. Kargar, N. R. Sesing, Z. Barani, T. T. Salguero, D. Yan, S. Rumyantsev, A. A. Balandin, *Adv. Electron. Mater.* **2023**, *9*, 2200860.
- [43] S. Baraghani, Z. Barani, Y. Ghafouri, A. Mohammadzadeh, T. T. Salguero, F. Kargar, A. A. Balandin, *ACS Nano* **2022**, *16*, 6325.
- [44] A. Mohammadzadeh, A. Rehman, F. Kargar, S. Rumyantsev, J. M. Smulko, W. Knap, R. K. Lake, A. A. Balandin, *Appl. Phys. Lett.* **2021**, *118*, 223101.
- [45] S. Ghosh, F. Kargar, A. Mohammadzadeh, S. Rumyantsev, A. A. Balandin, *Adv. Electron. Mater.* **2021**, *7*, 2100408.
- [46] M. Tadic, D. Nikolic, M. Panjan, G. R. Blake, *J. Alloys Compd.* **2015**, *647*, 1061.
- [47] N. Mironova-Ulmane, A. Kuzmin, I. Steins, J. Grabis, I. Sildos, M. Pärs, *J. Phys. Conf. Ser.* **2007**, *93*, 012039.
- [48] D. Dohy, G. Lucazeau, A. Revcolevschi, *J. Solid State Chem.* **1982**, *45*, 180.
- [49] T. Onuma, S. Fujioka, T. Yamaguchi, Y. Itoh, M. Higashiwaki, K. Sasaki, T. Masui, T. Honda, *J. Cryst. Growth* **2014**, *401*, 330.
- [50] C. Kranert, C. Sturm, R. Schmidt-Grund, M. Grundmann, *Sci. Reports* **2016**, *6*, 35964.
- [51] M. M. Lacerda, F. Kargar, E. Aytan, R. Samnakay, B. Debnath, J. X. Li, A. Khitun, R. K. Lake, J. Shi, A. A. Balandin, *Appl. Phys. Lett.* **2017**, *110*, 202406.
- [52] X. Xia, J. S. Li, C. C. Chiang, T. J. Yoo, F. Ren, H. Kim, S. J. Pearton, *J. Phys. D. Appl. Phys.* **2022**, *55*, 385105.
- [53] A. Almalki, L. Madani, N. Sengouga, S. Alhassan, S. Alotaibi, A. Alhassani, A. Almunyif, J. S. Chauhan, M. Henini, H. V. A. Galeti, Y. G. Gobato, M. P. F. De Godoy, M. B. Andrade, S. Souto, H. Zhou, B. Wang, M. Xiao, Y. Qin, Y. Zhang, *Mater. Today Electron.* **2023**, *4*, 100042.
- [54] S. L. Rumyantsev, A. P. Dmitriev, M. E. Levinshtein, D. Veksler, M. S. Shur, J. W. Palmour, M. K. Das, B. A. Hull, *J. Appl. Phys.* **2006**, *100*.
- [55] L. Dobrzanski, W. Strupinski, *IEEE J. Quantum Electron.* **2007**, *43*, 188.
- [56] H. Luo, X. Zhou, Z. Chen, Y. Pei, X. Lu, G. Wang, *IEEE Trans. Electron Devices* **2021**, *68*, 3991.
- [57] N. I. Bochkareva, A. M. Ivanov, A. V. Klochkov, Y. G. Shreter, *Semiconductors* **2019**, *53*, 99.
- [58] L. Li, Y. Shen, J. C. Campbell, *Sol. Energy Mater. Sol. Cells* **2014**, *130*, 151.